Geofísica Internacional (1997), Vol. 36, Num. 1, pp. 37-47

Tides and tidal currents in Ensenada de la Paz lagoon, Baja California Sur, Mexico

Francisco J. Sandoval[1] and José Gómez-Valdés
Centro de Investigación Científica y de Educación Superior de Ensenada, B.C., México.
[1] Present Address: Department of Oceanography, Florida State University, Tallahassee, USA.

Received: November 25, 1994; accepted: August 9, 1996.

RESUMEN

Se analizan datos de mareas y corrientes obtenidos en la laguna costera somera Ensenada de la Paz BCS, México. Se observa un incremento hacia la cabecera en las amplitudes de dos armónicas semidiurnas, así como diferencias de fase sobresalientes en todas las armónicas principales de la marea superficial. Sin embargo, se observa una disminución en la amplitud de la armónica de marea quincenal, con respecto a la boca. Se postula que la causa de este comportamiento es un balance entre el gradiente de presión superficial y la fricción con el fondo del tipo cuadrática. Los cambios en la marea superficial debidos a los efectos de la fricción con el fondo y a la configuración de la cuenca se examinan con un modelo hidrodinámico lineal. Las corrientes se pueden dividir en dos grupos: las típicas de un canal de mareas y las del interior lagunar, en donde las interacciones alineales parecen ser importantes. Se estima mediante un cálculo simple la importancia relativa de las interaccciones alineales de la corriente de marea residual.

PALABRAS CLAVE: Laguna costera, mareas, corrientes de marea.

ABSTRACT

Tides and tidal currents are observed in Ensenada de la Paz, a shallow coastal lagoon in Baja California Sur, Mexico. The amplitudes of two semidiurnal harmonics increase towards the head and there is a notably phase lag with respect to the mouth in the principal harmonics of surface tide. However, the amplitude of the fortnightly tide decreases toward the head. It is suggested that this behavior is caused by an approximate balance between surface pressure gradient and quadratic bottom friction. The influence of both bottom friction and basin configuration on surface tide are examined with a linear hydrodynamic model. Currents fall into two groups: a tidally-driven inlet flow and an interior flow wherein nonlinearities appear to be important. The relative importance of nonlinear interactions on tidal velocities is analyzed with a simple model.

KEY WORDS: Coastal lagoon, tides, tidal currents.

INTRODUCTION

In narrow coastal lagoons, adjacent ocean tides and tidal currents are the primary sources of mechanical energy. Dissipation of tidal currents is mainly due to bottom friction. In some cases, however, important momentum losses may occur due to flow separation effects. Bottom friction may play a dominant role in the tidal dynamics of rivers and shallow estuaries (LeBlond, 1978). Tidal processes may be dependent upon basin geometry, causing changes in mean sea level and long-term residual circulation. The evaluation of dynamical processes is complicated by nonlinearities (Carter *et al.*, 1979; LeBlond, 1991).

Shallow-water harmonic constituents result from the nonlinear interactions of tides and tidal flows with coastal topography (Dronkers, 1964). Overtides have frequencies which are multiples of the basic tidal components, for example, M_4 and M_6. Compound tides, on the other hand, are linear combinations of the basic tidal components; thus MS_f, a fortnightly-period harmonic, arises from M_2-S_2 interaction. These nonlinear features in sea level and tidal flows may produce flood/ebb asymmetries (Friedrichs and Aubry, 1988).

While advection may cause even overtides quadratic friction can generate odd overtides, semidiurnal compound tides and ter-, fifth-and sixth-diurnal compound tides (Parker, 1991). Murty *et al.* (1980) found important advective (inertial) terms in tidally-generated residual circulation in Masset Inlet and Masset Sound. Particularly in flow separation phenomena the inertial term may locally produce asymmetric residual circulation, residual eddies and second harmonics in the tidal current (Parker, 1991).

We present observations of tides and tidal currents in Ensenada de la Paz, a narrow, shallow lagoon located near the mouth of the Gulf of California. Field measurements of sea surface elevations and horizontal currents over three periods of 29 days each are reported. The influence of bottom friction and basin configuration on the surface tides is studied by means of a linear hydrodynamic model. A significant increase in the amplitudes of two semidiurnal harmonics, and phase lags in all the principal harmonics, were found between the basin head and the inlet. Nonlinear effects on tidal velocities are estimated with a simple model.

2. OCEANOGRAPHIC SETTING

The tides near the mouth of the Gulf of California are of mixed regime, like those of the North Pacific. The main constituents are M_2, S_2, K_1 and O_1 (Morales-Pérez and Gutierrez, 1989).

Bahía de la Paz is an embayment on the southwest coast of the Gulf of California at 24.1 to 24.8° N and

110.2 to 110.8° W. Depths range from 300 m at the inlet to 10 m at the head. Ensenada de la Paz is connected to Bahía de la Paz through an inlet 1.2 km wide, 4 km long and 7 m depth on average (Figure 1). The inner basin is shallower, with depths ranging from 6 m to 2 m. A channel reaches far into the lagoon. At mean sea level the surface area of the lagoon is approximately 45 km^2. The average tidal prism between low tide and the next high tide is approximately 50 x 10^6 m^3.

Morales and Cabrera-Muro (1982) estimated the flushing rate in Ensenada de la Paz at 31 x 10^6 m^3 per tidal cycle and the flushing time as 3.5 tidal cycles. They used a simple volume conservation model to reproduce the currents driven by tides and found good agreement with observations along the inlet. Two temperature time series over 8 months (October 1980-February 1981) were analyzed by Granados-Guzmán and Alvarez-Borrego (1984), who found that diurnal temperature fluctuations inside the lagoon were larger than semidiurnal fluctuations. In the channel the semidiurnal fluctuations exceeded the diurnal.

3. FIELD PROGRAM

Groups of Centro de Investigación Científica y de Educación Superior de Ensenada and Universidad Autónoma de Baja California Sur measured tides, currents, winds, salinity and temperature during November 1-29, 1980. Additional measurements were carried out from April 8 to May 9 of 1981 and between October 1 and October 30 of 1982 on the seasonal variability of velocity and density fields. A dye-dispersion experiment was also performed. The locations of the field measurements are shown in Figure 1.

Three KAHLSICO 310W A440 analog tide gauges were deployed, one outside of Ensenada de la Paz, another near the inlet-channel junction and the third at the head (stations T1, T2 and T3, respectively). One-hour samples were chosen for data processing. A permanent tidal station near the mouth of Ensenada de la Paz (station TIG), belonging to the Instituto de Geofísica at Universidad Nacional Autónoma de México, was also used.

Current velocities were recorded in November 1980 from stations E and G inside the lagoon; in April-May of 1981 at stations D, A1 and A2 near the point of channel separation and across the inlet; and in October of 1982 at station B near the inlet/channel connection. The current meter was suspended in the water column, close to the surface below low tide, except at mooring B which had two current meters. The current meters are ENDECO type 105 with a recording interval of 0.5 hour.

4. SURFACE TIDE DATA AND ANALYSIS

The sea level was checked with reference to station TIG by admittance analysis (Godin, 1991), and was found by

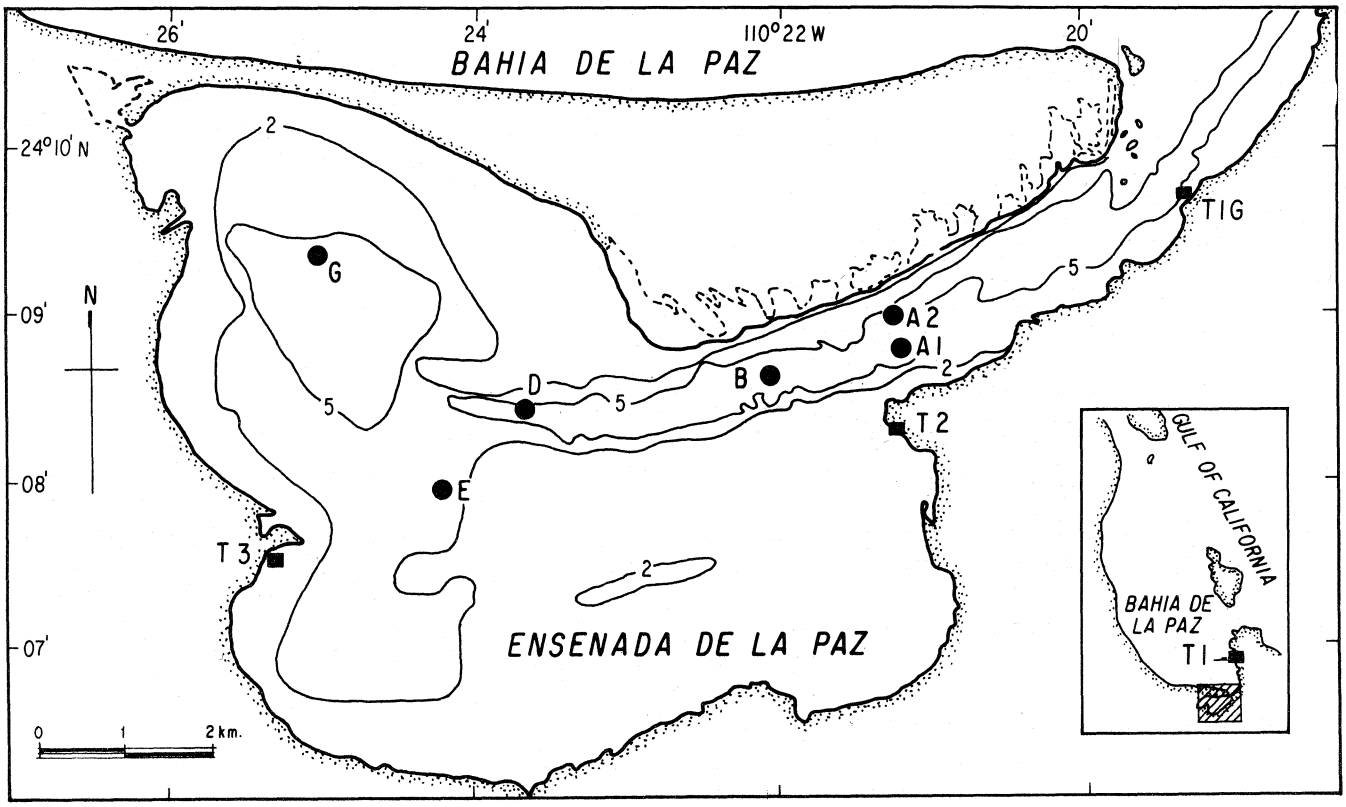

Fig. 1. Location and bathymetry of the coastal lagoon Ensenada de la Paz, BCS. Isobaths are in meters referred to mean sea level. □ = tide gauges, • = current meters.

this method to be appropriate for the purpose of this study. The type of tide is mixed, with semidiurnal behavior during spring tides and close to diurnal behavior during neap tides, as at the mouth of the Gulf of California. The average tidal range increases from 83 cm at T1 to 92 cm at T3 at spring tides, and decreases from 18 cm at T1 to 12 cm at T3 at neap tides.

Morales and Cabrera-Muro (1982) estimated the phase lag between T1 and T3 over 16.5 km and found 38 min at high tide (HW) and 76 min at low tide (LW), suggesting that the tidal wave traveled twice as fast at HW than at LW. The admittance phase lag for the diurnal (semidiurnal) band is estimated at 61 min (64 min).

The tidal height record has the general form

$$z(t) = z_0 + \sum_{k=1}^{R} A_k \cos(\sigma_k t - \alpha_k) + n(t), \qquad (1)$$

where $z(t)$ is the water level observed at a tidal station at time t, z_0 is the mean level, R is the number of constituents to be included in the fit, A_k and a_k are the kth amplitude and phase lag respectively, σ_k is the given frequency of the kth component and $n(t)$ is the residue. The (A_k, a_k) parameters are extracted from the records by least squares (Godin, 1972; Foreman, 1978). The expected error on the (A_k, a_k) pair can be calculated from

$$\pm\left(\frac{\epsilon}{\sqrt{N}}, \arcsin\frac{\epsilon}{|A_k|\sqrt{N}}\right), \qquad (2)$$

where ϵ is the standard deviation of the residue and N is the number of hourly observations (Godin, 1972).

Table 1 displays amplitude and Greenwich phase lag of the principal tidal components for TIG and T3. Tide gauges are about 11 km apart; record length is from April 8 to May 9, 1981. We assume a constant Rayleigh criterion of 1 in the determination of the harmonic constituents, which gives a frequency range of 0 to 0.322 cycles/hour and results in the inclusion of 29 constituents, 14 from the potential of the tide generating force and 15 shallow-water constituents. The amplitude gain and the phase difference are computed at the basin head with respect to the entrance. The amplitudes of M_2 and S_2 increase by 1.8 cm and 1.7 cm respectively. Significant phase differences are found in K_1 (8 ± 4°), M_2 (15 ± 4°) and S_2 (16 ± 5°). The harmonic analysis for 1980 and 1982 (not shown), is consistent with Table 1.

In addition to the components in Table 1, some shallow-water components, resulting from M_2, S_2 and K_1, show up inside the lagoon. The fortnightly component MS_f decays about 3±1 cm. MK_3, SK_3 and MS_4 components are not significant outside the lagoon but reach amplitudes of 1.7, 2.1 and 1.4 cm respectively at T3.

Table 1

Amplitude (A) and phase (θ) of the principal tidal components for the Bahía la Paz (TIG) and Ensenada de la Paz (T3). Record length is from 14:00 hrs on April 8 to 11:00 hrs on May 8 of 1981. Phase angles in GMT; time zone Z=+7. Maximum expected errors are shown at 95% confidence limits

	TIG		T3	
	A (cm)	θ(°)	A (cm)	θ(°)
O_1	16.9 ± 0.9	180 ± 4	16.5 ± 1.0	185 ± 5
K_1	23.2 ± 0.9	169 ± 3	23.2 ± 1.0	177 ± 3
N_2	5.6 ± 0.9	118 ± 12	5.9 ± 1.0	127 ± 13
M_2	23.7 ± 0.9	117 ± 3	25.4 ± 1.0	133 ± 3
S_2	21.0 ± 0.9	116 ± 3	22.7 ± 1.0	132 ± 3

5. CURRENTS

Near-surface currents were measured during 29-day periods in November of 1980 at E and G stations and in late April and early May of 1981 at A1, A2 and D1 stations. Low-frequency currents, of periods longer than two days were removed by applying a low-pass filter $A_{48}A_{48}A_{49}/(48^2 \times 49)$ (Godin 1972).

The velocity components at station G, the innermost station from the entrance, are shown in Figure 2. The velocities are typically of 4 cm s^{-1} for spring tides (days 8 and 21) and 2 cm s^{-1} for neap tides (day 15). The low-frequency velocity component was small with an apparent fortnightly oscillation in a preferred northeast direction. The velocities were irregular during neap tides.

The East-West current u at station E (Figure 3) is larger than the North-South current v, e.g., 5 cm s^{-1} versus 3 cm s^{-1} at spring tides. The low-frequency u component is near 3 cm s^{-1} with a marked fortnightly oscillation towards the East. It is larger than the correspondent v component. Ebb velocities (u-positive) are higher than flood velocities (u-negative). The maximum near-surface current is approximately 8 cm s^{-1}.

The u-component at station D is larger than the v-component (Figure 4). Maximum u-velocities are 40 cm s^{-1} at spring tides (April 18 and May 3) and 20 cm s^{-1} at neap tides (April 25). A similar rectilinear current is observed at station A1 (Figure 5). Typical velocities are 50 cm s^{-1} at spring tides and 20 cm s^{-1} at neap tides. The maximum ebb current peaked at about 65 cm s^{-1}. Ebb velocities are comparatively stronger than flood velocities at this site. The opposite occurs at station A2: flood velocities exceed those of ebb, and the maximum flood current is close to 60 cm s^{-1}.

5.1 Rotary spectral estimates

The rotary spectrum of complex-valued velocity series (Mooers, 1973) is defined by the vector sum

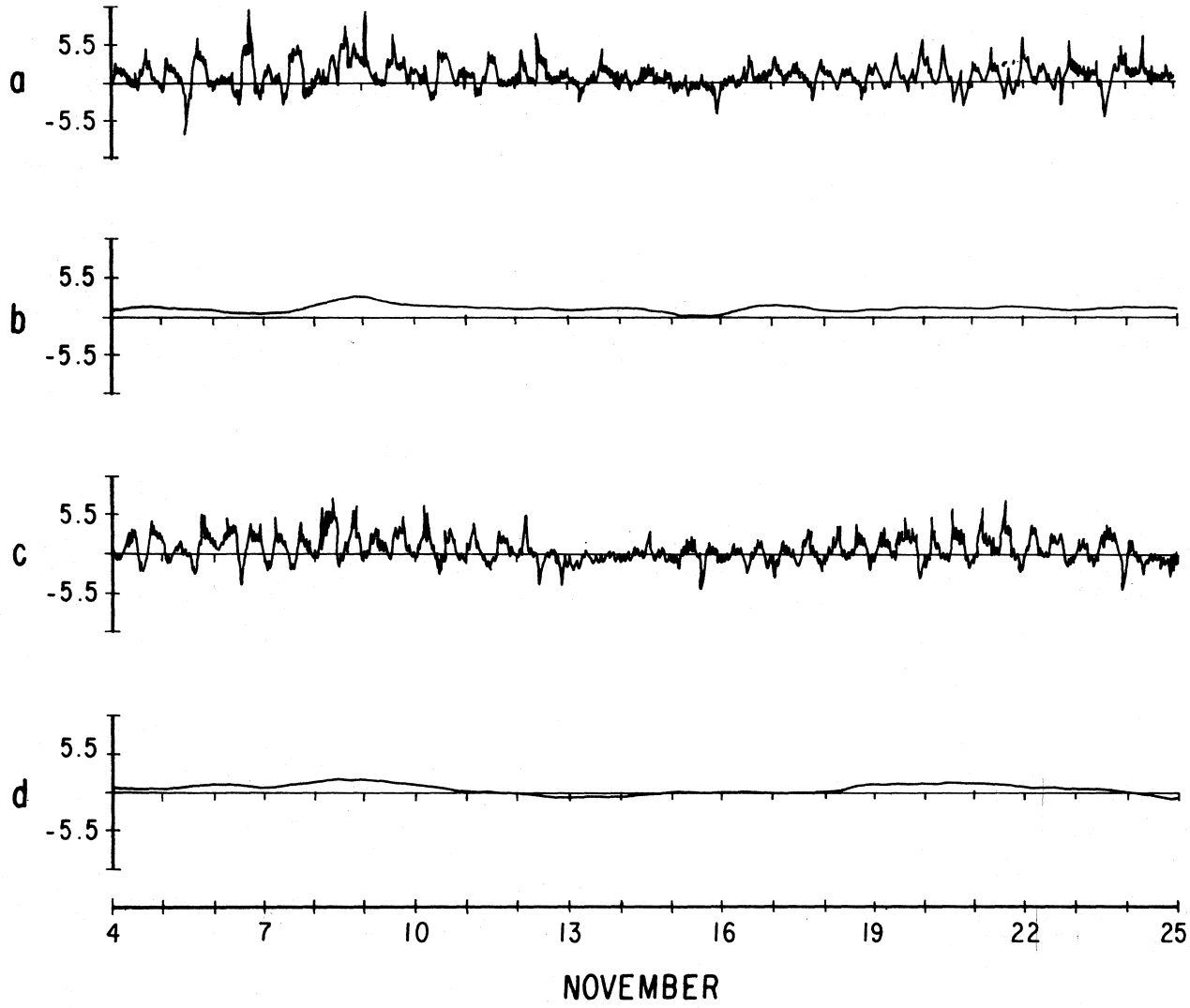

Fig. 2. Current at station G in November 1980. (a) North-South v component, (b) low-passed v component, (c) East-West u component, and (d) low-passed u component.

$$\mathbf{w}_k(t) = \sum_{k=-\infty}^{\infty} \mathbf{w}_k \exp(i\sigma_k t), \qquad (3)$$

where a positive value of k corresponds to anticlockwise rotation of two complex rotary vectors, each of magnitude $|\mathbf{w}_k|$ and phase angle $\alpha=\sigma_k t$. The representation can be either harmonic or spectral. The current ellipse parameters are the semimajor axis $\mathbf{M}_k = |\mathbf{w}_k| + |\mathbf{w}_{-k}|$, the semiminor axis $\mathbf{m}_k = |\mathbf{w}_k| - |\mathbf{w}_{-k}|$, and the inclination of the major axis $\theta_k = (\alpha_k + \alpha_{-k})/2$. The estimate of the inner rotary spectrum (Mooers, 1973) for a resolution of 1 cycle/day (0.0417 cycles/hour) is shown in Table 2. Stations G and E show a significant fraction of the energy in the low-frequency and high-frequency bands but most of the energy density at stations A1, A2 and D is concentrated in semidiurnal and diurnal bands.

Table 3 displays current ellipse parameters. For stations E and G, the semidiurnal and diurnal bands were rota-

Table 2

Inner rotary spectra of the current measurements for a resolution of 1 cycle/day. The estimates are shown in percentage of total energy relatively over four frequency bands. Low-frequency means periods longer than two days and high-frequency periods smaller than 1/2 day. G, E, D, A1 and A2 are the current meter stations.

Station	Low-frequency	Diurnal	Semidiurnal	High-frequency
G	24	13	39	24
E	9	10	64	17
D	1	10	85	4
A1	1	11	86	2
A2	1	9	87	3

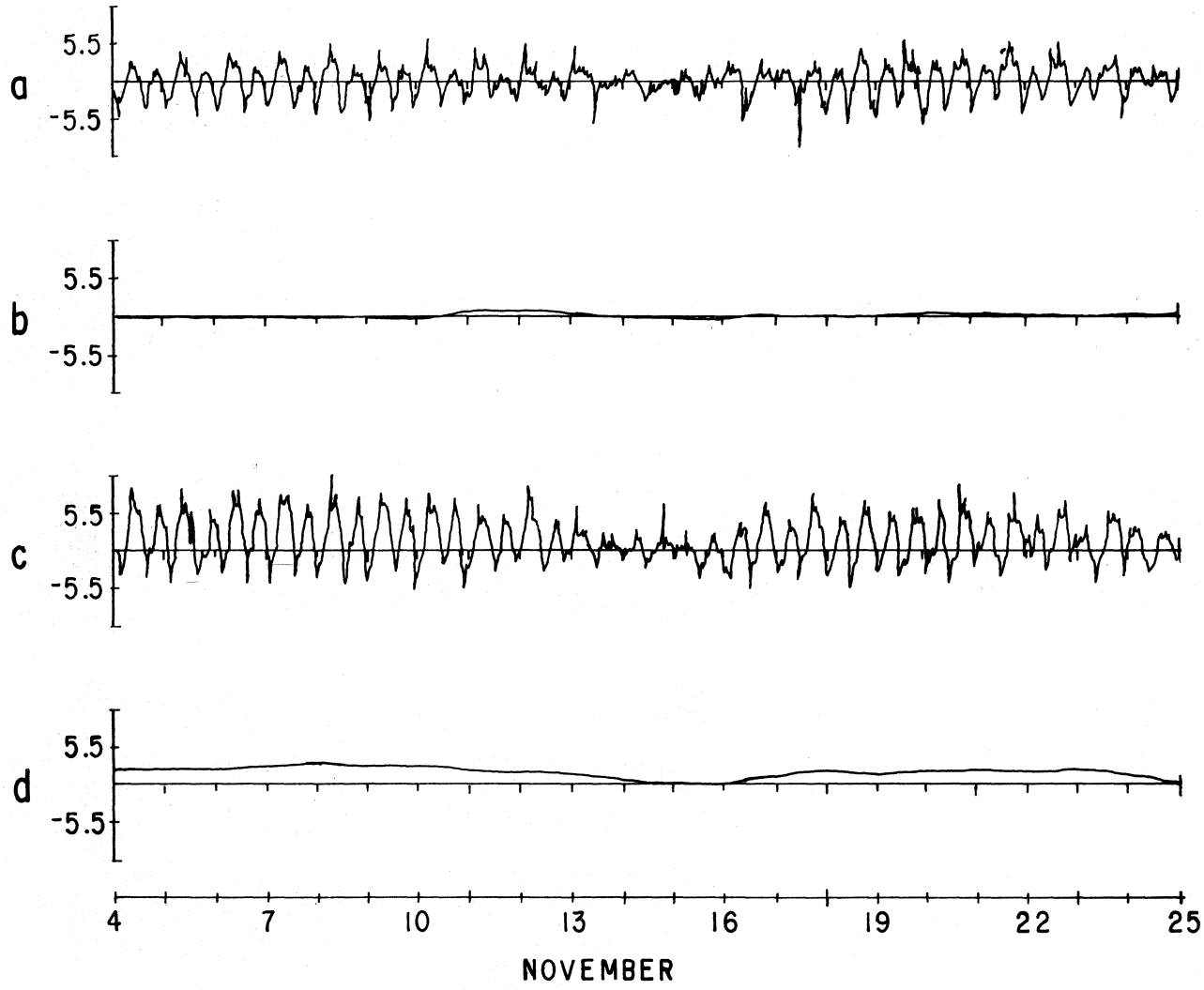

Fig. 3. As in Fig.2, station E.

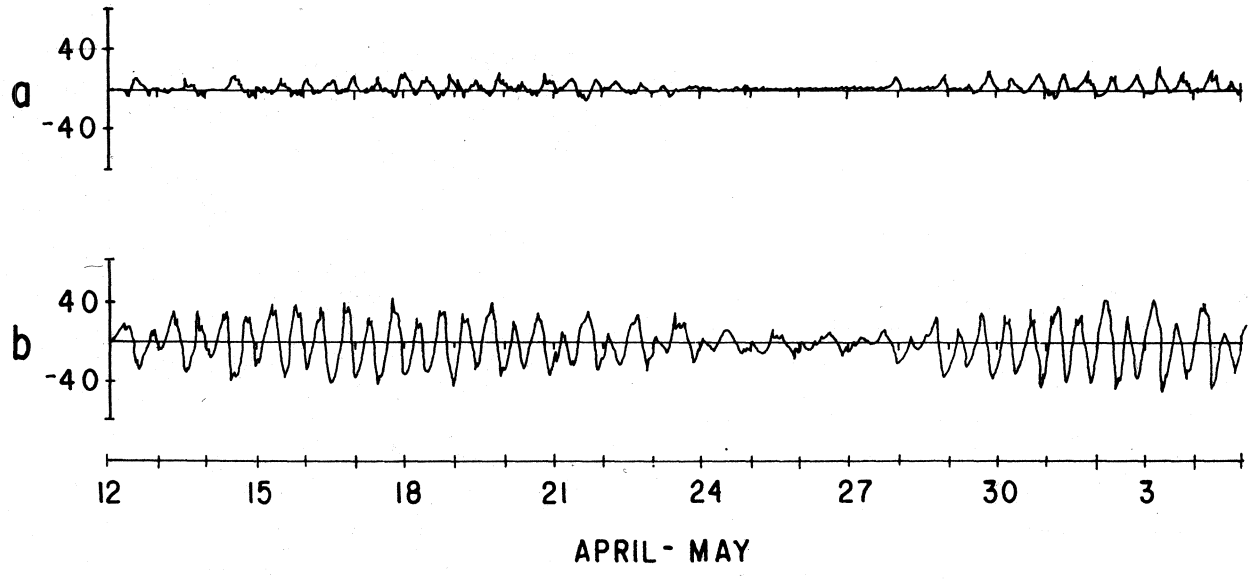

Fig. 4. Current at station D in April-May of 1980. (a) v component, (b) u component.

Table 3

Spectral estimates of ellipse parameters for the currents for a resolution of 1 cycle/day. M is the semimajor axis in cm s^{-1}, m is the semiminor axis in cm s^{-1} and θ is the (trigonometric) inclination of major axis in degrees. G, E, D, A1 and A2 are the observational sites

		M	m	θ
band 0				
	G	1.9	0.3	220
	E	1.6	0.2	186
	D	3.0	-0.1	133
	A1	4.0	0.3	186
	A2	4.8	-0.6	129
band 1				
	G	1.4	-0.1	110
	E	1.7	-0.1	217
	D	9.2	0.7	167
	A1	16.4	-0.8	184
	A2	13.9	0.8	201
band 2				
	G	2.3	-0.8	145
	E	4.3	0.7	210
	D	26.4	0.2	168
	A1	45.7	0.3	184
	A2	42.2	0.5	200

tional, ellipticity O (10^{-1}). The diurnal current rotated clockwise and the low-frequency current rotated anticlockwise at both stations. At site E the semidiurnal band rotated anticlockwise; at G, it rotated clockwise. The semidiurnal and diurnal tidal currents were strongly polarized, ellipticity O (10^{-3}), at stations D, A1 and A2.

Table 4 shows the total correlation between the current meter data and the predicted tide at station TIG. The current stations along the inlet and channel bed were highly correlated with the surface tide at the entrance of the lagoon, as expected. However, the diurnal current at sites E and G were weakly correlated with the ocean tide. This shows that diurnal streams are small in the lagoon.

6. ROLE OF BOTTOM FRICTION AND BASIN GEOMETRY

We assume a one-dimensional linear model with a linear friction law and we neglect the Earth's rotation and basin curvature. The lagoon is modelled as an open rectangular channel connected to a closed square basin of uniform depth (Figure 6).

6.1 First approximation

The nonrotating approximation is reasonable because the Rossby radius of ≈ 128 km, is nearly 21 times the lateral dimension of the basin. Curvature effects associated with the inlet and the channel bed were also neglected (Liu, 1987; Rocha and Clarke 1987). The condition for Bragg scattering resonance is $2k\Lambda^{-1}= 1$, where k is the wavenumber of the incident wave and Λ that of the boundary curvature. For $k \approx 0.02$ km^{-1} and $\Lambda \approx 0.63$ km^{-1}, this effect need not be considered since $2\,k/\Lambda$ is much smaller than unity.

6.2 The model

The vertically integrated equations of motion on the assumption of a harmonic time-dependence (Dronkers, 1964) are

$$-i\sigma u + ru = -g\frac{\partial \eta}{\partial x}, \tag{4}$$

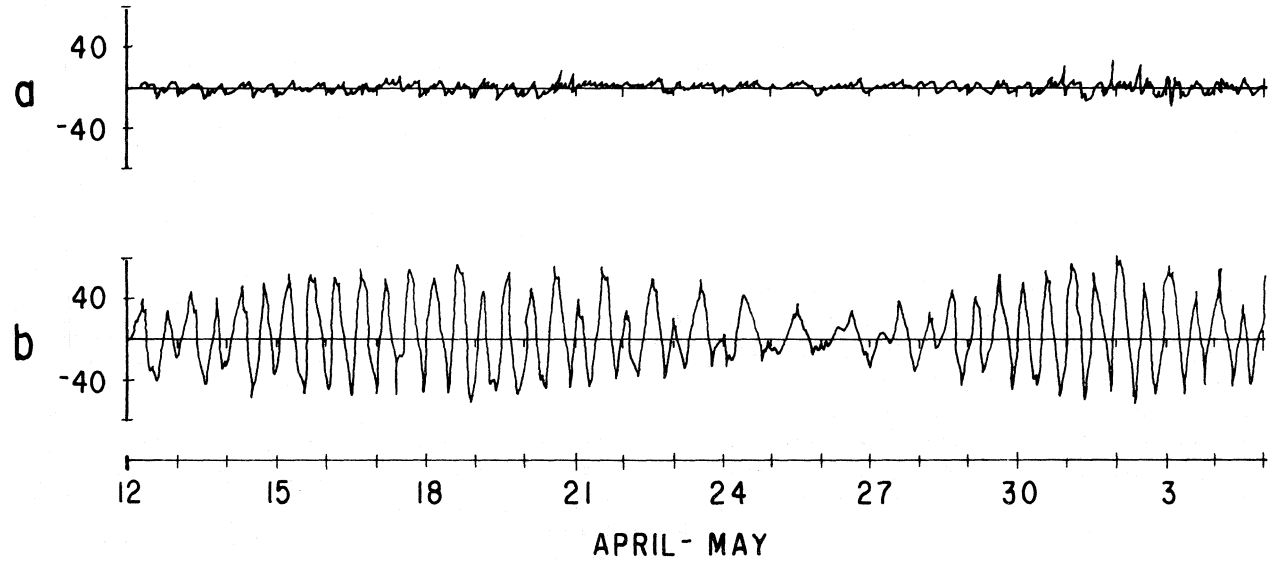

Fig. 5. As in Fig. 4, station A1.

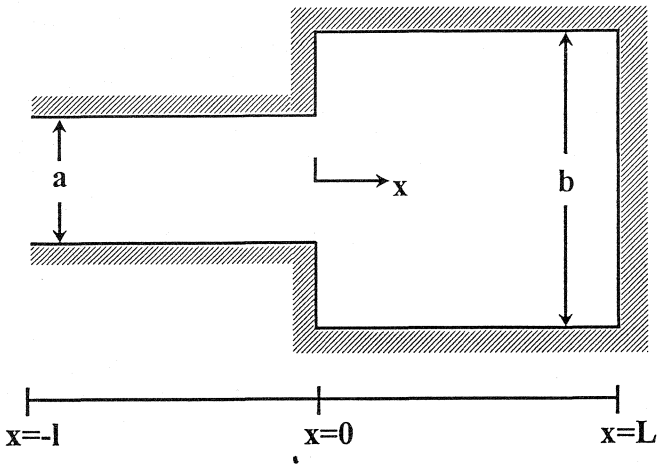

Fig. 6. A sketch of basin configuration.

Table 4

Total correlation coefficients between current measurements and predicted tide at TIG for the two principal tidal bands for a resolution of 1 cycle/day. G, E, D, A1 and A2 are the current meter stations.

	G	E	D	A1	A2
band 1	0.57	0.71	0.97	0.98	0.94
band 2	0.84	0.95	0.99	0.99	0.99

$$-i\sigma\eta + h\frac{\partial u}{\partial x} = 0, \tag{5}$$

where η is the vertical displacement of the water surface, u is the vertically integrated velocity in the along-channel direction x, r is a bottom stress resistance coefficient, g is the acceleration due to gravity, h is the water depth in the undisturbed state, σ is the angular frequency. The water is considered to be of constant density under static equilibrium and the surface stress is assumed negligible for the motions of interest.

We now obtain

$$\frac{\partial^2\eta}{\partial^2 x} + k^2(1+i\tilde{r})\eta = 0, \tag{6}$$

where k is the incident wavenumber, $\tilde{r} = r/\sigma$ and $\sigma = k\sqrt{gh}$. Surface elevation is known at the entrance, here prescribed as $\eta^- = \eta_0 \exp(-i\sigma t)$ at $x^- = -l$; surface elevation and mass flux are continuous across the junction, $\eta^- = \eta^+$; and $(Su)^- = (Su)^+$ as $x \to \pm 0$, S being the cross-sectional area. Also, there is no normal mass flux at the end of the basin, $u^+ = 0$ at $x^+ = L$. The reference frame is centered at the junction for simplicity; the rightward variables are denoted by $(\cdot)^+$ and the leftward variables by $(\cdot)^-$.

The surface elevation relative to the entrance is

$$\eta(x) = \begin{cases} (\cos Kx + A\sin K(l+x)/\cos Kl, & \text{if } x < 0, \\ B\cos K(L-x), & \text{if } x > 0, \end{cases} \tag{7}$$

with $A = \omega B \sin Kl$, $B = (\cos Kl \cos KL - \omega \sin Kl \sin KL)^{-1}$, $K = \kappa + i\mu$ with $\kappa = K[(1+\tilde{r})^{1/2} + 1]^{1/2}2^{1/2}$, $\mu = k[(1+\tilde{r})^{1/2}-1]^{1/2}/2^{1/2}$, and $\omega = b/a$; a is the width of the inlet on the negative side and b is the (wider) matched basin on the positive side.

Two special cases can be found from the analytic solution: a semiclosed rectangular channel by setting $\omega \to 1$, and a frictionless response by replacing in either case $K \to k$, i.e., $\kappa = k$ and $\mu = 0$. The presence of friction ultimately determines the complex form of the solution. It implies an additional phase shift inside the basin with respect to the incoming wave at the opening. If friction is omitted, one obtains a zero phase lag anywhere within the basin relative to the entrance.

Because Kl, KL and μ/κ are smaller than unity, a simple approximation of amplitude and phase difference may be found from a first-order Taylor's expansion. The approximate solutions are obtained for the basin head with respect to the entrance. Thus, the amplitude response simplifies to

$$\eta(L)/\eta(-l) \sim 1 + \omega\kappa l\kappa L, \tag{8}$$

and the phase difference to

$$\varphi(L) - \varphi(-l) \sim 2\,\omega\mu\kappa lL, \tag{9}$$

since $\omega\kappa l\kappa L \ll 1$.

This approximation suggests that the amplitude ratio excludes the damping parameter as a (first-order) contribution. The spatial scale of the undamped traveling wave is related to the basin geometry. The width ratio determines the magnitude of the other dimensionless parameters (i.e., κl and κL both of O (10^{-1})), and the amplitude increases for smaller waves, i.e., M_2 and S_2. A numerical computation suggests that higher frequency waves have greater lags. For a semiclosed rectangular channel phase differences may increase by one order of magnitude, due to the factor 2ω.

6.3 Comparison with observations

Figure 7 shows amplitude and phase differences for the two significantly enlarged components M_2 and S_2. Significant increases in amplitude are only expected to occur near the basin head relative to the entrance, thus comparisons are made at sites TIG and T3. Average amplitudes and phase lags are computed with respect to TIG. The length scales in the model were w = 6.25, l = 5 km, L = 7 km and h = 6. These values were selected by examining different sizes close to those of the actual basin.

The model was designed to fit the amplitudes of Table 1. It was assumed that the amplitude response is primarily due to the effect of basin configuration as theory suggests that the influence of bottom friction is nearly absent. All principal harmonic constituents were considered. Two overall friction coefficients, suitable for the diurnal and semidiurnal frequency bandwidths, have been used in de-

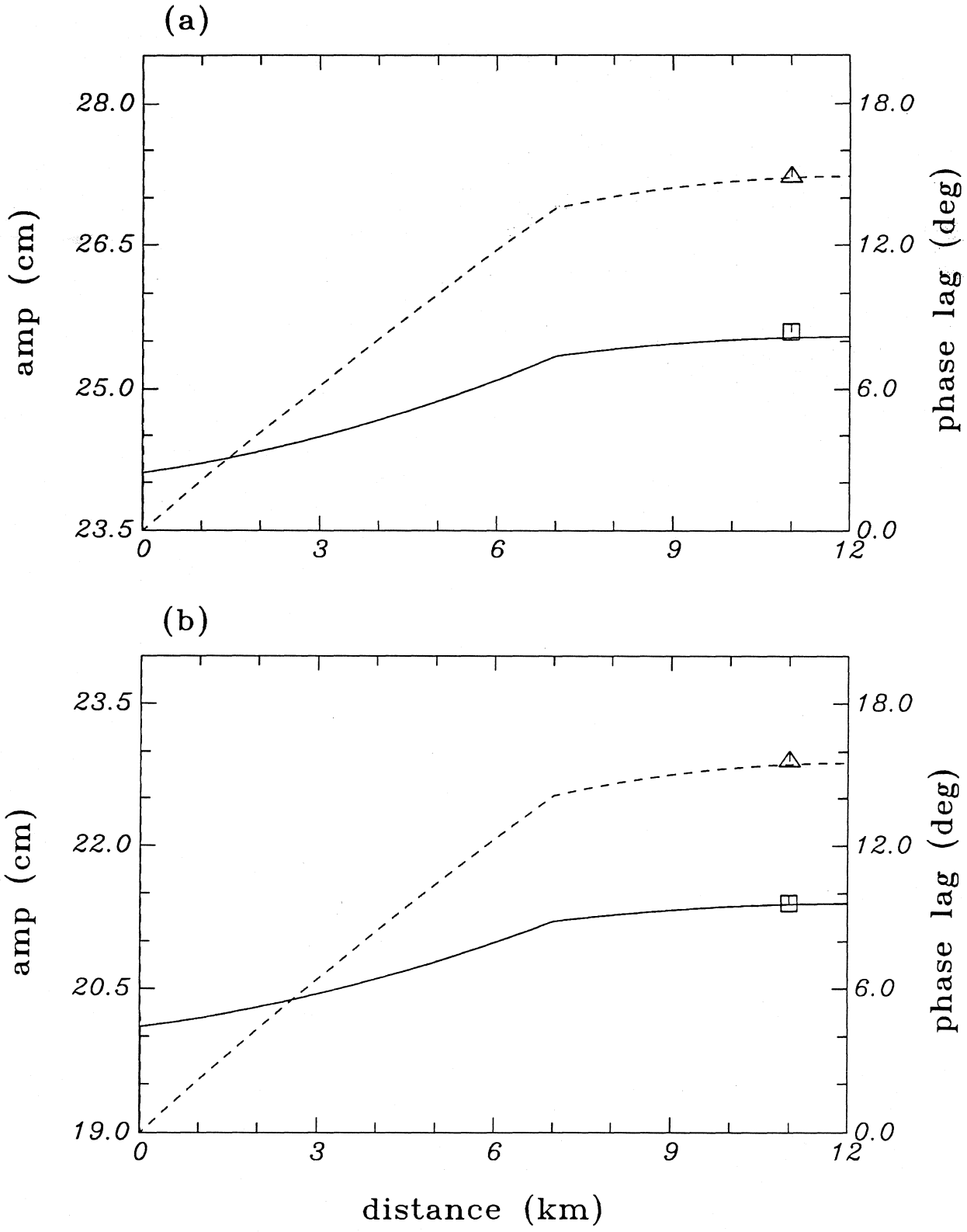

Fig. 7. Theoretical amplitude (solid) and phase lag (dashed) versus along-channel distance for the tidal components M_2 (a) and S_2 (b). The friction coefficient is $r = 4.0 \times 1^{-4}\ s^{-1}$ for both components. The harmonically analyzed surface tide data are shown by: □ (amplitude) and △ (phase lag).

termining the scales of the model. We have explored the sensitivity to variations in depth which appears to be of minor importance.

Friction coefficients were refined by best fit to the phase lags of Table 1. Friction coefficients for the two major tidal harmonics were found to be $\tilde{r} = 6.04$, $r = 4.4 \times 10^{-4}$ s^{-1}, for K_1 and $\tilde{r} = 2.85$, $r = 4.0 \times 10^{-4}$ s^{-1}, for M_2. Significant relative increases were confirmed for the amplitudes of M_2 and S_2 at the head with respect the entrance. Phases lag more at the higher frequencies.

7. NONLINEAR ASPECTS OF TIDAL CURRENTS

Current measurements were analyzed according to Godin (1972) and Foreman (1978). The results were expressed in terms of the current ellipse parameters. Next, the amplitude of the significant shallow-water components was normalized by the product of the amplitudes of the input source components.

Table 5 shows the relative importance of nonlinear interactions on the residual tidal components. The figures are ratios of semimajor axes: the significant shallow-water components divided by the product of the astronomical components. The 95% confidence limits corresponding to the significant shallow-water components (not shown here) were determined after Godin (1983).

Notice a sustained increase in order of magnitude as one progresses from inlet stations toward the innermost station. Second-order compound harmonics seem to dominate. Third-order harmonics, $2MK_6$, M_6, $2MS_6$, and $2SM_6$, dominate only at E and particularly at G, where diurnal currents are weak and frictional effects seem be of importance.

Table 5

Relative importance of shallow-water tidal components with respect to their astronomical components. Only those shallow-water components significant at 95% confidence limits are shown. G, E, D, A1 and A2 are the current meter stations

	G	E	D	A1	A2
MO_3	4.1×10^{-3}		1.8×10^{-2}	5.2×10^{-3}	9.4×10^{-3}
MK_3	2.8×10^{-1}		1.1×10^{-2}	4.5×10^{-3}	5.9×10^{-3}
SK_3	5.2×10^{-1}	1.9×10^{-2}	2.0×10^{-2}	6.4×10^{-3}	1.1×10^{-3}
MN_4			1.3×10^{-2}		
M_4		4.3×10^{-2}	5.9×10^{-3}	1.7×10^{-3}	3.0×10^{-3}
S_4			5.7×10^{-3}		
$2MK_5$	1.9×10^{-1}	3.3×10^{-2}	4.0×10^{-4}		
M_6		8.6×10^{-3}		3.2×10^{-5}	
$2MS_6$		7.2×10^{-3}	1.0×10^{-4}	2.8×10^{-5}	3.3×10^{-5}
$2SM_6$			1.0×10^{-4}	2.8×10^{-5}	3.3×10^{-5}

It appears that these third-order harmonics may be generated primarily by a quadratic frictional mechanism (Dronkers, 1964; Godin and Gutiérrez, 1986). If diurnal flow advection plays a minor role at site G, the ter-diurnal compound tides, MO_3, MK_3 and SK_3, may be due to effects of continuity and/or coupling of elevation to bottom friction (higher-order momentum loss).

Walters and Werner (1991) have suggested that the nonlinear source mechanisms for the quarter-diurnal harmonics M_4, MN_4 and MS_4 may be continuity, local advection and depth effect on bottom friction in that order. Flow separation phenomena are known to be of local importance and may cause even overtides and quarter-diurnal compound tides (Mei *et al.*, 1974; Parker, 1991). Since we have found MN_4 and S_4 to be conspicuous and semidiurnal, these harmonics could be caused by inertial separation effects.

8. DISCUSSION

We have found a small but significant increase in the amplitudes of the semidiurnal harmonics M_2 and S_2, and important phase lags in all the harmonics. These changes in the surface tide of the lagoon are found at the head with respect to the entrance. They are attributed to bottom friction and basin configuration. Damping in amplitude should normally occur but amplification may also occur depending on the length of the incoming wave and the dimensions of the lagoon. In agreement with observations, our theoretical model accounts for the major features of the local surface tide.

The fitting coefficients of linear friction, r, and quadratic drag, C_D, are related by $r = C_D\,|u| / (h + \eta)$. If we take $r = 4.0 \times 10^{-4}$, $|u| = \frac{1}{2}$ (45) cms^{-1}, $h = 6$ m and $\eta = 25$ cm, an estimate of C_D is found to be O (10^{-2}), an order of magnitude larger than its typical value. Thus the effect of bottom friction should be large in narrow, shallow lagoons. However, the influence of bed roughness on C_D remains to be investigated. Also, the quadratic parameterization of tidal friction may lead to harmonic distortion, modulation and rectification, and to the emergence of multiplet harmonics at sub- and supra-tidal frequencies (Gallagher and Munk, 1971).

The amplitude decrease in the fortnightly component MS_f at the end of the basin relative to the entrance may balance the form $g < \partial\eta/\partial x > = -C_D < u|u| > /h$, where $<\cdot>$ denotes a time average over the record length. An order-of-magnitude estimate yields drop $|\Delta\eta| = O$ (1 cm) per 10 km length, assuming that the residual subtidal velocity is O(10 cm s^{-1}). Thus reduction in the amplitude MS_f may be due to a nonlinear equilibrium between quadratic bottom friction and surface pressure gradient. Surface elevations between the bay and the inlet suggest an amplitude modulation in the spring-neap cycles, probably as a result of a nonlinear frictional effect. Clarke (1990) solved numerically the time-dependent balance outlined above, using the interacting constituents M_2 and S_2 as an incident doublet in the surface pressure term. He found that the nonlinear

solution is smaller at large velocities and larger at small velocities. The nonlinear bottom stress retarding the flow was more coherent than the linear bottom stress retarding the flow with the velocity field. When comparing the linear and nonlinear solutions, his findings suggest that quadratic frictional effects may cause an amplitude modulation in the fortnightly cycles of tides and tidal currents. The current velocities at the inlet vary with the surface tide at the entrance of the lagoon. Spectral estimates provide representative values of 85% for semidiurnals and 10% for diurnal tides. A residual analysis suggests that 93% of the semidiurnal tides and 90% of the diurnal tides can be harmonically represented by the primary components. This explains why the one-dimensional continuity model of Morales and Cabrera-Muro (1982) is appropriate. Granados-Guzmán and Alvarez-Borrego (1984) also reported temperature fluctuations driven by this tidal pattern.

The analysis of current velocities suggests a mixed, tidally-induced inlet flow, modified by asymmetrical expansion/contraction of the width of basin and spreading of the channel bed deep inside the basin. When tidal flows interact with a significant variation in basin geometry, important contributions to the dynamic balance may result, leading to shallow-water harmonic components through nonlinear interactions (LeBlond, 1991).

The residual analysis of currents shows that for station E, 67% of the diurnal variance and 85% of the semidiurnal, and for current station G, 40% of the diurnal variance and 68% of the semidiurnal, can be represented by the primary components. Nonlinearities and perhaps ambient and measurement noises may be significant in the residual variance of current measurements. Bottom friction, wave drift and local inertial effects may be the dominant processes controlling the nonlinear dynamics of the residual tidal variance. Our study documents the relevance of nonlinear interactions in Ensenada de la Paz.

We suggest that subtidal residual circulation is produced by basin configuration as the inlet/channel bed junction is asymmetric. The lateral velocity distribution in the neighborhood of the junction is modulated by the spring and neap tidal cycles. Flow rectification may occur by advection and friction, and local inertia dominates for the ebb-flood asymmetry. The flow is first weakened near the edge of the southwest side of the inlet, and moves closer to the inlet junction. Near the junction the flow would be stronger on the northern side and weaker on the southern side; afterwards it rotates clockwise north of the inlet and counterclockwise in the southern and central area due to spreading of the channel bed. At ebb tide the southern waters are close to the channel junction resulting in a stronger ebb flow around the edge of the southwest side of the passage which causes a velocity shear across the neighborhood of the junction.

ACKNOWLEDGMENTS

The observational program was performed under grants by SEP and CONACYT, Mexico. The group of Coastal Lagoons at CICESE and Ocean Science at UABC carried out the field work. FJS received partial financial support from the U.S. Department of Energy, Contract No. DE-FG05-92ER61416. JGV was partially supported by CONACYT under Grant 3523-T. We are indebted to Allan J. Clarke, George L. Weatherly and Dietmar Müller for their valuable insight and stimulating discussions. Dong-Ping Wang, Salvador F. Farrreras and Silvio G. Marinone provided helpful suggestions to an early version of this manuscript. We thank Ignacio González for processing the tidal records and Rodrigo Nuñez for drawing Figure 6. Special thanks go to Mia Shargell for her editorial review of the paper. Two anonymous reviewers provided constructive criticism which led to improvement of the manuscript.

BIBLIOGRAPHY

CARTER, H.H., T.O. NAJARIAN, D.W. PRITCHARD and R.E. WILSON, 1979. The dynamics of motion in estuaries and other coastal water bodies. *Rev. Geophys. Space Phys., 17*, 1585-1590.

CLARKE, A. J., 1990. Application of a frictional channel flow theory to flow in the Prince of Wales Channel, Torres Strait. *J. Phys. Oceanogr., 20*, 890-899.

DRONKERS, J. J., 1964. Tidal Computations in Rivers and Coastal Waters. North-Holland Publishing Company, Amsterdam. 518 pp.

FOREMAN, M. G. G., 1978. Manual for tidal currents analysis and prediction. Pac. Mar. Sci. Rep. 78-6. Institute of Ocean Sciences, Victoria, British Columbia. 70 pp.

FRIEDRICHS, C. T. and D. G. AUBREY, 1988. Nonlinear tidal distortion in shallow well-mixed estuaries. A synthesis. *Estuarine. Coastal and Shelf Sci., 27*, 521-545.

GALLAGHER, B. S. and W. H. MUNK, 1971. Tides in shallow water: Spectroscopy. *Tellus, 23*, 346-363.

GODIN, G., 1972. The Analysis of Tides. University of Toronto Press, Toronto. 264 pp.

GODIN, G., 1983. The Spectra of point measurements of currents: their features and their interpretation. *Atmos. Ocean. 21*, 263-284.

GODIN, G., 1991. The analysis of tides and currents. *In:* Tidal hydrodynamics, B.B. Parker, Ed. John Wiley & Sons, New York, 675-709.

GODIN, G. and G. GUTIERREZ, 1986. Nonlinear effects in the tide of the Bay of Fundy. *Cont. Shelf Res., 5*, 379-402.

GRANADOS-GUZMAN, A. and S. ALVAREZ-BORREGO, 1982. Variabilidad de temperatura en la

Ensenada de la Paz, BCS. *Ciencias Marinas, 9*, 133-141.

LEBLOND, P. H., 1978. On tidal propagation in shallow rivers. *J. Geophys. Res., 83*, 4717-4721.

LEBLOND, P. H., 1991. Tides and their interactions with other oceanographic phenomena in shallow water. *In:* Tidal Hydrodynamics, B.B. Parker, Ed., John Wiley & Sons, New York, 357-378.

LIU, P.L.F., 1987. Resonant reflection of water in a long channel with corrugated boundaries. *J. Fluid Mech., 179*, 371-381.

MEI, C. C., P. L. F. LIU and A. T. IPPEN, 1974. Quadratic head loss and scattering of long waves. *J. Waterway Harbors Coastal Eng. Div., ASCE, 100*, 217-239.

MOOERS, C. N. K., 1973. A technique for the cross spectrum analysis of pairs of complex-valued time series, with emphasis on the properties of polarized components and rotational invariants. *Deep-Sea Res., 20*, 1129-1141.

MORALES, E. R. and H. R. CABRERA-MURO, 1982. Aplicación de un modelo numérico unidimensional a la Ensenada de la Paz, BCS. *Ciencias Marinas, 8*, 69-89.

MORALES-PEREZ, R. A. and G. GUTIERREZ, 1989. Mareas en el Golfo de California. *Geofís. Int., 28*, 25-46.

MURTY, T. S., F. G. BARBER and J. D. TAYLOR, 1980. Role of advective terms in tidally generated residual circulation. *Limnol. Oceanogr., 25*, 529-533.

PARKER, B. B., 1991. The relative importance of the various nonlinear mechanisms in a wide range of tidal interactions: *In:* Tidal hydrodynamics, ed. Parker, B.B. John Wiley & Sons, New York, 237-268.

ROCHA, C. A. and A. J. CLARKE, 1987. Interaction of ocean tides through a narrow single strait and narrow multiple straits. *J. Phys. Oceanogr., 17*, 2203-2218.

WALTERS, R. A. and F. E. WERNER, 1991. Nonlinear generation of overtides, compound tides, and residuals. *In:* Tidal hydrodynamics, ed. Parker, B.B. John Wiley & Sons, New York, 297-320.

Francisco J. Sandoval[1] and José Gómez-Valdés
Centro de Investigación Científica y de Educación Superior de Ensenada, B.C., México. A. P. 2732., Km 107 Carret. Tijuana-Ensenada, Ensenada, B.C., Mex.
[1] Present Address: Department of Oceanography, Florida State University, Tallahassee, FL 32306-2048, USA.